Estimating Helicopter Noise Abatement Information with Machine Learning

Eric Greenwood
Aeroacoustics Branch
NASA Langley Research Center
Hampton, VA

ABSTRACT

Machine learning techniques are applied to the NASA Langley Research Center's expansive database of helicopter noise measurements containing over 1500 steady flight conditions for ten different helicopters. These techniques are then used to develop models capable of predicting the operating conditions under which significant Blade-Vortex Interaction noise will be generated for any conventional helicopter. A measure for quantifying the overall ground noise exposure of a particular helicopter operating condition is developed. This measure is then used to classify the measured flight conditions as noisy or not-noisy. These data are then parameterized on a nondimensional basis that defines the main rotor operating condition and are then scaled to remove bias. Several machine learning methods are then applied to these data. The developed models show good accuracy in identifying the noisy operating region for helicopters not included in the training data set. Noisy regions are accurately identified for a variety of different helicopters. One of these models is applied to estimate changes in the noisy operating region as vehicle drag and ambient atmospheric conditions are varied.

NOTATION

A	Rotor disc area, ft^2 (m^2).
a_0	Ambient speed of sound, ft/s (m/s).
b	Support vector hyperplane intercept.
C	Support vector "soft margin" penalty weight.
c_i	Class of the i^{th} data member $\in \{-1, 1\}$.
C_T	Main rotor thrust coefficient. $T/\left(\rho_0 A\Omega^2 R^2\right)$
C_W	Main rotor weight coefficient. $W/\left(\rho_0 A\Omega^2 R^2\right)$
f	Effective flat plate drag area, ft^2 (m^2).
I_G	Gini impurity index.
$k(\vec{x}, \vec{x}')$	Weighting function.
L_A	A-weighted Sound Pressure Level, dBA.
$\bar{L}_A$	Average A-weighted Sound Pressure Level, dBA.
L_{AE}	A-weighted Sound Exposure Level, dBA.
L_{AG}	Ground Noise Exposure Level, dBA.
M_H	Main rotor hover tip Mach number. $\Omega R/a_0$
N	Number of samples in the bin.
N_b	Number of main rotor blades.
N_{False}	Number of samples that fail the criterion.
N_{True}	Number of samples that pass the criterion.
p_i	Probability of randomly selected data sample being a member of a class chosen randomly in accordance to the probability distribution of samples in the bin.
R	Rotor radius, ft (m).
T	Thrust, lbf (N).
T_0	Reference integration time, s.
t	Time of observation, s.
V	Ground speed, knots (km/h).
V_0	Reference ground speed, knots (km/h).
V_{CAS}	Calibrated airspeed, knots (km/h). $V\sqrt{\rho_0/\rho_{SL}}$
W	Weight, lbf (N).
$\vec{w}$	Support vector hyperplane unit normal vector.
w_{ij}	Weight of the j^{th} connection to the i^{th} neuron.
$\vec{x}$	Feature space.
x_i	Misclassification of the i^{th} data member.
$\vec{x}_i$	Location the i^{th} data member in the feature space.
α	Main rotor tip-path-plane angle of attack, rad. (deg.).
γ	Flight path angle, rad. (deg.).
λ_i	Induced inflow ratio.
μ	Main rotor advance ratio.
$\vec{\nu}$	Augmented feature space.
ρ_0	Ambient air density, slug/ft^3 (kg/m^3).
ρ_{SL}	Ambient air density at sea level, slug/ft^3 (kg/m^3).
σ	Radial basis function scale parameter.
ϕ	Nonlinear kernel function.
ψ	Rectified linear unit activation function.
Ω	Main rotor rotational speed, rad./s.

Presented at the American Helicopter Society 74th Annual Forum, Phoenix, Arizona, USA, May 14–17, 2018.

Helicopters serve to support a number of useful roles within the community, such as electronic news gathering and aerial photography, inspection and maintenance of power lines, police and emergency medical services, aerial cranes, cropdusting, civil transport, and sightseeing. However, community acceptance of these operations is limited by the resulting noise. For instance, voluntary restrictions on helicopter operations have recently been adopted in the Los Angeles and New York City areas to increase community acceptance (Refs. 1–3). The acoustic impact of civil helicopter operations will need to be reduced in order to allow for a greater variety and volume of helicopter operations in the future. In the long term, design changes such as reduced tip speeds or the widespread adop-

tion of active and passive rotor noise reduction technologies may result in significant reductions in the noise emitted by future helicopters. However, because the noise radiated by helicopters is extremely sensitive to the helicopter's operating state, immediate noise reductions can be achieved through the development of low noise flight procedures applicable to the existing civil fleet.

Since 1981, the Helicopter Association International (HAI) has published "Fly Neighborly" (Ref. 4) guidance intended to provide helicopter operators with effective methods to reduce helicopter noise impacts on communities and increase public acceptance of helicopter operations. The Fly Neighborly guidance includes general techniques for reducing community noise impacts, such as avoiding noise sensitive areas or flying at a higher altitude, as well as advice on developing more specific noise abatement procedures that avoid noisy flight conditions unique to the type of helicopter flown. While community noise levels during quiet (e.g., cruise) flight conditions may be dominated by tail rotor noise sources, the primary cause of the most objectionable—i.e., "noisy"—flight conditions is main rotor Blade-Vortex Interaction (BVI).

The operational conditions determined to cause BVI noise are often displayed in the Fly Neighborly guidance using a "fried egg" plot. A fried egg plot, derived from noise measurements of a typical light helicopter, is shown in Fig. 1. The high BVI noise region is shaded on the plot and is defined in terms of indicated airspeed and rate of climb. The operator can use this information to develop noise abatement procedures that avoid the BVI noise region, such as the proposed quiet approach highlighted in red on the plot. This approach starts with a steep descent at constant speed, followed by decreasing airspeed at a high rate of sink to pass below the high BVI noise region, resembling a Category A approach for FAA Part 29 (transport category) rotorcraft.

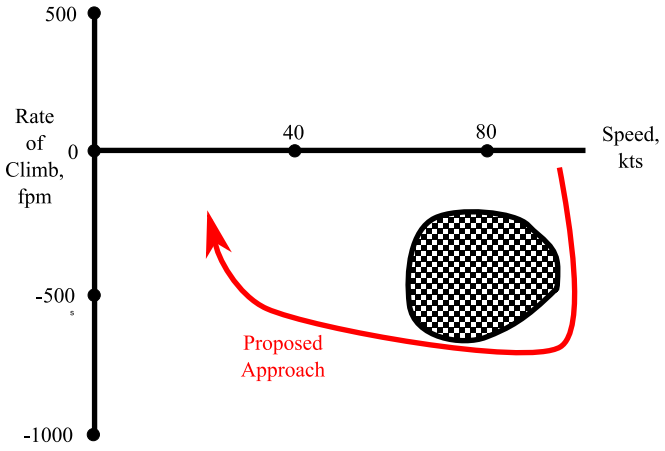

Fig. 1: A representative fried egg plot with a proposed noise abatement approach trajectory shown in red. (Adapted from Ref. 4.)

The data normally used to generate the fried egg plot are intended to be collected by the helicopter's manufacturer and the resulting noise abatement guidance provided to operators in an optional supplement to the aircraft's flight manual. However, due to the difficulty of collecting these data, detailed noise abatement guidance is not routinely provided for new helicopters. When such guidance is still provided, it is often based on measurements or subjective identification of noisy conditions from inside the vehicle. However, it is now known that due to the directional nature of BVI noise, noise levels heard inside the cabin are not representative of noise radiated toward the ground (Ref. 5). Even when comprehensive ground noise measurements are conducted, they are usually limited to steady flight conditions at a particular test location and vehicle configuration, which may not be representative of the actual BVI noise radiation characteristics of the helicopter when flown under a different set of ambient conditions, gross weight, or fuselage drag (Refs. 6, 7).

The NASA Langley Research Center—often in collaboration with other US Government agencies, industry, and academia—has collected ground noise data for a wide variety of helicopter types, from light commercial helicopters to heavy military utility helicopters. Many of these data have been collected and processed to generate helicopter source noise descriptions in the form of Rotorcraft Noise Model (RNM) (Refs. 8, 9) hemispheres describing the frequency, magnitude, and direction of helicopter noise as a function of the vehicle's flight condition. While this database is expansive, it covers only a fraction of helicopter types in current commercial and military service and was measured under a limited set of ambient conditions and vehicle configurations. The objective of this paper is to combine this helicopter noise database with the principle of nondimensionalization and modern machine learning techniques in order to develop models capable of estimating the noisy operating states of any conventional helicopter. These models should be capable of providing noise abatement information specific to the ambient atmospheric atmospheric conditions in which the vehicle operates and variations in the vehicle's drag or gross weight, e.g., that caused by the installation or removal of mission equipment.

APPROACH

The approach used in this paper to build the helicopter noise abatement information models consists of several steps:

1. Convert noise data for each vehicle into a form describing the ground noise levels of the vehicle as a function of flight condition.

2. Classify the flight conditions of each vehicle into noisy and not-noisy conditions.

3. Nondimensionalize the main rotor operating conditions for all measured vehicles and combine them into a single general database.

4. Use machine learning techniques to train a model on a subset of the database in order to identify noisy conditions.

5. Apply the classifier to estimate the probability of a noisy condition over the range of nondimensional parameters defining the rotor operating condition.

6. Use the probabilistic model output to identify regions of dimensionally-defined flight conditions that are likely to be noisy for a specific helicopter operating under a specific set of ambient conditions.

7. Validate the model against measured noise data excluded from the initial training set.

The data used to build the model in this paper include measurements of the MD Helicopters MD-902 and Mil Mi-17 collected during Acoustics Week III at Eglin Air Force Base (AFB) in 2007 (Ref. 10), the Bell 430 helicopter collected during the NASA/Bell/Army Maneuver Acoustics Flight Test at Eglin AFB in 2011 (Ref. 11), the Airbus AS350BA collected at Salton Sea, Amedee Army Airfield (AAF), and Sweetwater USMC Auxiliary Airfield during the NASA/Army Altitude Variation Test from 2014-2015 (Ref. 12), the Robinson R-44 and R-66 helicopters collected in Phase I of the NASA/FAA/Army joint test conducted in September 2017 at Eglin AFB, and the Airbus AS350B3, Airbus EC130B4, Bell 206L3, and Bell 407 helicopter collected in Phase II of the NASA/FAA/Army joint test conducted in October 2018 at Amedee AAF. These data have been processed to generate a database of source noise hemispheres including 1560 different flight conditions. The helicopters included in the noise database, their maximum takeoff gross weights, main rotor blade numbers, and the test sites where data were collected, are tabulated in Table 1. The helicopter types included in the database range from light to medium weights with a variety of rotor systems, including two-bladed teetering rotors, multibladed articulated rotors, and multibladed hingeless rotors.

Table 1: Table of helicopters included in database.

Type	Max Takeoff Gross Weight (lbf)	N_b	Test Site
Airbus AS350BA	4630	3	Various
Airbus AS350B3	4960	3	Amedee AAF
Airbus EC130B4	5351	3	Amedee AAF
Bell 206L3	4150	2	Amedee AAF
Bell 407	5400	4	Amedee AAF
Bell 430	9300	4	Eglin AFB
Mil Mi-17	28660	5	Eglin AFB
MD Helicopters MD-902	6500	5	Eglin AFB
Robinson R-44	2500	2	Eglin AFB
Robinson R-66	2700	2	Eglin AFB

Ground Noise Metric Development

To convert this collection of source noise hemispheres into fried egg plots for each vehicle, a representative ground noise level must be generated for each flight condition in the acoustic database. A stereographic projection of the A-weighted noise levels over one source noise hemisphere is shown in Figure 2a for the MD-902 helicopter in a 950 fpm (-9° flight path angle) descent at 60 knots. High levels of BVI noise are radiated ahead of and slightly toward the retreating side of the helicopter for this operating state. The out-of-plane noise levels, defined in this paper as the noise radiated 30° or more below the plane of the horizon, are then propagated to a ground plane 1500 ft below the helicopter using straight ray propagation, including attenuation due to spherical spreading and atmospheric absorption. The ground noise levels, L_A, for the MD-902 are plotted in Figure 2b for the same hemisphere shown in Figure 2a. Although noise levels generally attenuate toward the edges of the ground noise footprint, the occurrence of BVI causes noise levels to peak in a localized region ahead of the helicopter.

One measure of the resulting "noisiness" of the flight condition is the mean A-weighted sound pressure level propagated to the ground plane. The flight condition can then be classified as noisy if the mean A-weighted ground noise level is in the upper 35% of the range of mean ground noise levels calculated for that vehicle. Figure 3a shows the resulting fried egg plot for the MD-902. Each measured flight condition is represented with a filled circle marker: the red markers represent those classified as noisy and the black those that are not. The noise level contours are interpolated from the mean ground noise levels associated with each condition, showing that for this helicopter in the tested configuration, the noisy flight conditions occur at steep descent rates and moderate airspeeds. However, this measure of noisiness does not account for the increased annoyance due to the increased duration of sound exposure during lower speed flight. The Sound Exposure Level (SEL), L_{AE}, integrates the total acoustic energy of a flyover, and is expressed by the following:

$$L_{AE} = 10\log_{10}\frac{1}{T_0}\int_{t_0}^{t_1} 10^{L_A(t)/10}dt \qquad (1)$$

where T_0 is a reference time interval, typically defined as one second, and the interval $[t_0, t_1]$ defined as the times where noise levels are within 10 dBA of the peak level recorded during the flyover.

Calculating the SEL requires a time history of L_A. While the time history could be simulated using the noise hemispheres for each flight condition, this reduces the generality of the measure as it requires a specific flight trajectory to be associated with that flight condition. However, a generic duration correction can be developed to account for variations in speed proportional to the change L_{AE} with speed for any flight trajectory by

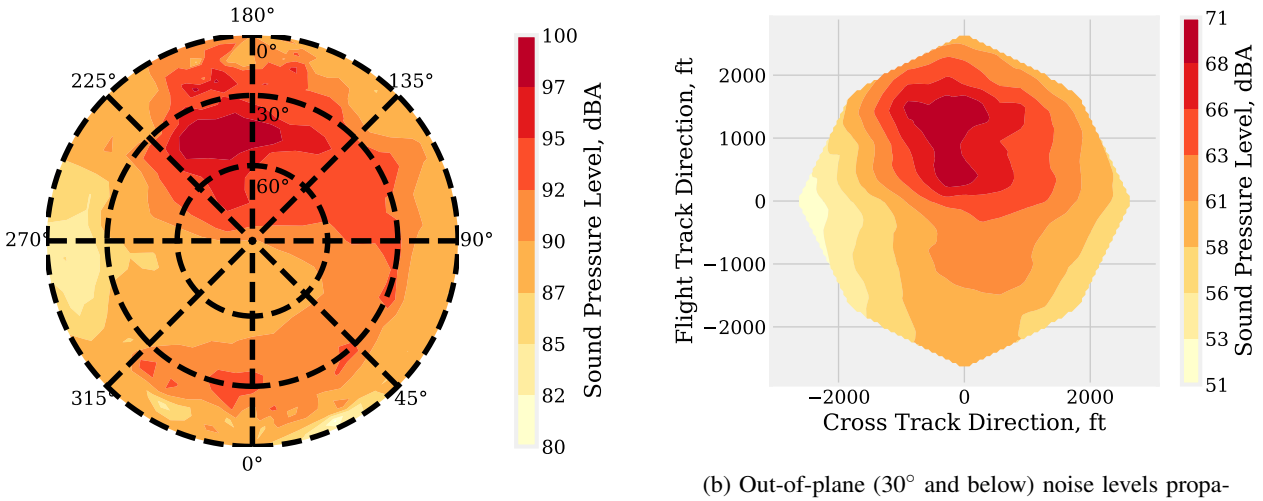

(a) Stereographic (top-down) projection of noise source hemisphere. Nose at 180° azimuth.

(b) Out-of-plane (30° and below) noise levels propagated to ground plane for 1500 ft altitude above ground level.

Fig. 2: Source noise hemisphere (a) and propagated ground noise levels (b) for MD-902 helicopter in a 60 knot, 950 fpm descent.

recognizing that:

$$L_{AE} \approx 10\log_{10}\sum_i 10^{L_{A_i}} + 10\log_{10}\frac{T}{T_0} \tag{2}$$

for a constant time interval, T.

Therefore, a representative Ground Noise Exposure Level, L_{AG}, can be defined for a constant speed, V, as:

$$L_{AG} \equiv \bar{L}_A + 10\log_{10}\frac{V_0}{V} \propto \bar{L}_{AE} \tag{3}$$

given a reference speed, V_0. The value of V_0 is arbitrary, defining only the airspeed at which no correction is applied, and will be set to 60 knots in this paper. The resulting fried egg plot for the MD-902 generated using this metric is shown in Figure 3b. Accordingly, the noisy region shifts toward lower speeds, where the duration effect increases the noise levels. This new metric causes four conditions at high speed to be reclassified as not-noisy and two conditions at low speed to be reclassified as noisy compared to the metric without a duration correction shown previously in Figure 3a.

Data Conditioning

Next, the data generated for all of the helicopters must be represented on a common basis suitable for interpretation by the machine learning algorithms. It has been shown in previous research that the main rotor BVI noise of helicopters is governed by a set of four nondimensional parameters (Ref. 13). By expressing the main rotor operating condition in a nondimensional form, the experimental noise data may be generalized across a wide range of dimensionally-defined operating states, at least for the same rotor geometry. In this paper, the main rotor operating state is defined by the tip-path-plane angle of attack (α), advance ratio (μ), weight coefficient (C_W), and hover tip Mach number (M_H), with the aim of collapsing the data across dissimilar rotor systems. In additional to these parameters, the number of rotor blades (N_b) influences the specific operating conditions at which intense BVI noise occurs. These five parameters (α, μ, C_W, M_H, N_b) are used as the "features" that the machine learning algorithms use to identify noisy operating conditions.

It is well established that for a certain set of parameters, μ, C_W, M_H, and N_b, the BVI noise will reach a peak value at a certain main rotor tip path plane angle of attack, α, where the miss-distance between the vortices and the blades is small, and will diminish for angles of attack greater or less than that value (Ref. 5). For the heavier helicopters in the database, it is often impossible to safely achieve rates of sink high enough to reach angles of attack, α, greater than the peak value for BVI noise. In order to realistically enclose the noisy region for these heavier helicopters, synthetic not-noisy points are added to the acoustic database at angles of attack 6° greater than the maximum included in the measured data across the range of advance ratios, μ, and at the average values of M_H and C_W measured for that particular helicopter.

Of the 1560 steady operating conditions included in the database, 213 were identified as noisy. Consequently, the majority (not-noisy) class is represented by approximately 7:1 over the minority (noisy) class in the data. Most machine learning methods will be biased toward the majority class when the data are imbalanced in this way. Several methods exist to compensate for this imbalance. One method that was found to successfully correct the bias in this data set is called the Synthetic Minority Over-sampling TechniquE (SMOTE) (Ref. 14). SMOTE generates additional synthetic members of the minority class that are quasirandomly inserted nearby other existing members of the minority class. Figure 4 plots the measured data points for the MD-902 along the angle of attack (α) and advance ratio (μ) feature dimensions. Once again, red markers represent data that are classified as noisy and black those that

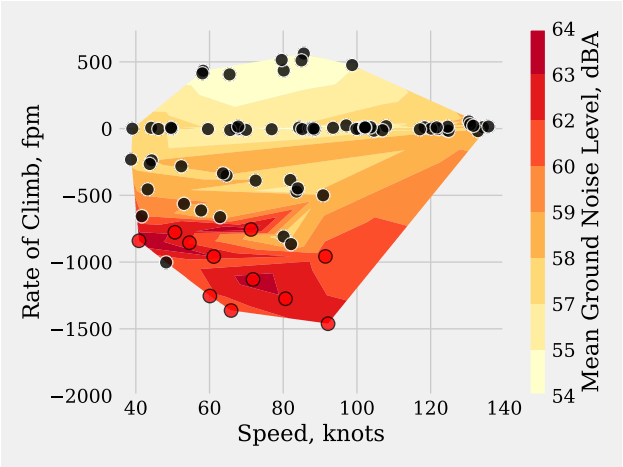

(a) Mean ground noise level contours without duration correction.

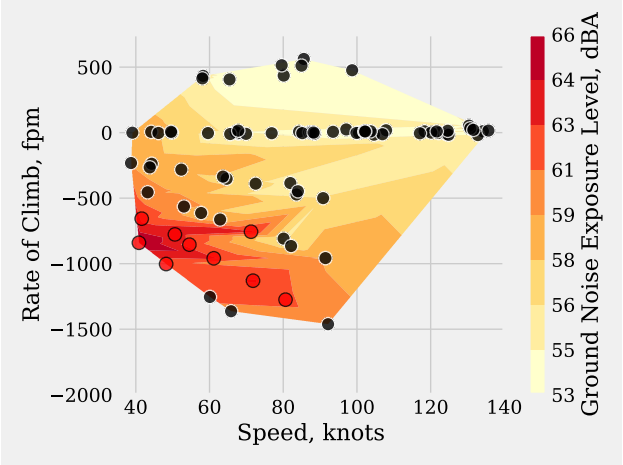

(b) Ground noise exposure level contours accounting for sound exposure due to duration effect.

Fig. 3: Ground noise level plots for the MD-902 generated using measured data from Acoustics Week III at Eglin. Measured flight conditions for each metric are marked with circles: black circles were identified as quiet and red circles as noisy.

are not. The blue markers are synthetic noisy samples that have been generated by the SMOTE technique, filling in the noisy region that is sparsely sampled in the measured data, and equalizing the number of data points in each class. Finally, scale bias is removed from the data before applying machine learning methods by scaling the feature values across the entire data set across a range of negative two to two, so that the mean value and range of each of the features is equal. For clarity, this scaling is not applied when plotting the data in the following figures.

Machine Learning Technique Evaluation

Several machine learning methods were evaluated and are listed in Table 2. Each of these classifiers is available in the open source Python package scikit-learn (Ref. 15), which provides a uniform interface to a large number of machine learning methods. This modularity allows a number of methods to be

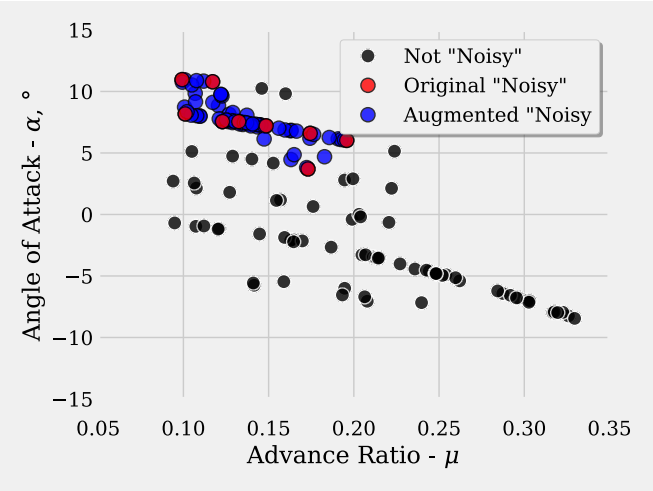

Fig. 4: Balancing the minority (noisy) class using the Synthetic Minority Oversampling TechniquE (SMOTE).

evaluated as a part of the same process. Each of the methods was applied to the database, with the MD-902 data withheld for later validation that the model has capability to predict the noisy region of the operating envelope for a helicopter not included in the training data set. The accuracy of the model was assessed on the remaining data using a 5-fold cross validation method. The data were randomly divided into five equally sized partitions. Each model was fit to data from four of the five partitions, and the accuracy of the classification model validated against predictions for the excluded partition. This process was repeated for all five possible excluded partitions, and accuracy scores averaged to produce a single 5-fold cross validation accuracy score. The wall clock time required to fit and validate the model in this manner on a twelve core workstation (2.5 GHz per core) is also tabulated.

Table 2: Table of machine learning methods evaluated, with cross-validation accuracy and fitting time assessed on dataset with MD-902 data withheld.

Machine Learning Method	5-fold Cross Validation Accuracy (%)	Wall Clock Model Fitting Time (s)
Support Vector Machine	82.2	16.0
Random Forest	80.9	0.625
Multilayer Perceptron	82.9	9.6
Gaussian Process	83.1	51500
Naïve Bayes	73.5	0.01

The five methods all achieve fairly good accuracy on the conditioned data, although the Naïve Bayes approach, which builds a probabilistic model under the assumption that the features are

independent, is notably less accurate than the other four methods. The Gaussian Process approach also builds a probabilistic model, but the dependence between features is accounted for during the model fitting. This is done by fitting the model to the posterior probability distribution of the data. While the method is accurate, the model fitting time is extensive in comparison to the other methods. For these reasons, the Naïve Bayes and Gaussian Process models are not assessed further in this paper in favor of the Support Vector Machine, Random Forest, and Multilayer Perceptron classifiers.

Support Vector Machine

The Support Vector Machine (SVM) approach aims to identify a hyperplane that divides points in the feature space belonging to one class from another (Ref. 16). The hyperplane is chosen to maximize the margin between the hyperplane and the closest member of each class, i.e.,

$$\min_{\vec{w},\vec{b}} ||\vec{w}|| \tag{4}$$

such that the hyperplane with unit normal, $\vec{w}$, and intercept, $\vec{b}$, divides the points $\vec{x}_i$ in accordance with their class, $c_i \in \{-1,1\}$:

$$c_i(\vec{w}\cdot\vec{x}_i - \vec{b}) \geq 1 \tag{5}$$

In practice, it is not often possible to define a hyperplane that cleanly separates all members of one class from another. To account for this, a "soft margin" condition is added, which allows, but penalizes members of, one class being on the "wrong" side of the hyperplane.

The Support Vector Machine fitting problem can then be expressed with the "soft margin" as:

$$\min_{\vec{w},\vec{b},\xi} \frac{1}{2}||w||^2 + C\sum_i \xi_i \tag{6}$$

subject to:

$$c_i(\vec{w}\cdot\vec{x}_i - \vec{b}) \geq 1 - \xi_i \tag{7}$$

where ξ_i are measures of the degree to which points, $\vec{x}_i$, are misclassified, and C is a tunable parameter that controls the relative importance of maximizing the margin (small C) versus minimizing misclassification (large C).

Very often, it is difficult to separate members of one class from another with a linear function. For example, Figure 5 plots the line (i.e., a two-dimensional hyperplane) dividing data classified from measurements of the Robinson R-66, where the noisy region is surrounded by points that are not-noisy.

A common method of extending linear classification methods to nonlinear problems is the "kernel trick" (Ref. 17), which maps the feature space $\vec{x}$ to a linear combination of nonlinear kernels:

$$k(\vec{x},\vec{x}') = \langle \phi(\vec{x}), \phi(\vec{x}') \rangle \vec{v} \tag{8}$$

where $\vec{v}$ is the augmented feature space.

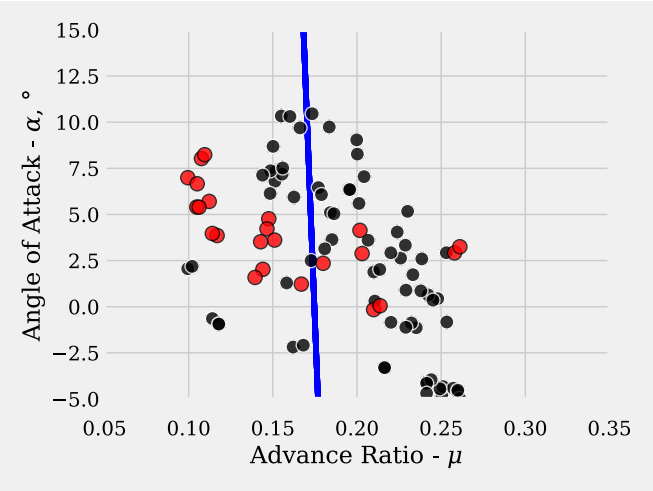

Fig. 5: Poor division (blue line) of classified conditions for the Robinson R-66 helicopter using a linear Support Vector Machine.

For example, by using an exponential radial basis function kernel with a tunable parameter σ of the form:

$$\phi = \exp(-\sigma||\vec{x}-\vec{x}'||) \tag{9}$$

the R-66 data points can be mapped to a new higher dimensional feature space, $\vec{v}$, as shown in Figure 6, that allows a linear hyperplane, shown in blue, to more effectively divide the noisy and not-noisy members from each other. The tunable parameters, C and σ, are set in the paper using a grid search method to identify the parameter combination that achieves the best 5-fold cross-validated accuracy.

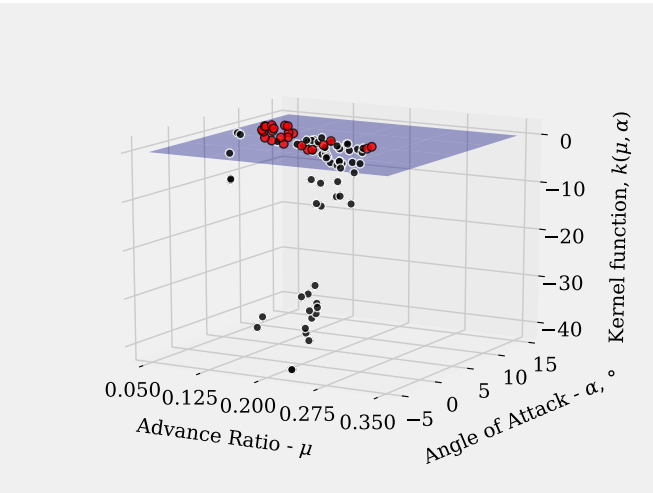

Fig. 6: Improved division (blue plane) of classified conditions for the Robinson R-66 helicopter using a Support Vector Machine with an exponential radial basis function kernel.

Although the SVM classifier is a nonprobabilistic classifier method, the Platt scaling (Ref. 18) technique can be used to transform the classifier output to estimate the probability of

a noisy condition across the nondimensional feature space of the model. Platt scaling works by fitting a logistic regression model to the classifier accuracy scores as the model is trained. Figure 7a shows the estimated probability of a noisy condition as a function of rotor angle of attack and advance ratio, where the other parameter values match those associated with the MD-902 data set. Superimposed on the probability contours are the measured data points, categorized in red for noisy and black for not-noisy, as in Figure 3. The high probability of noisy conditions region agrees well with those conditions from the measured data that were identified as noisy. The noisy region includes all nine conditions identified from the measured data as noisy, and four conditions identified as quiet. Those conditions that are more likely to be noisy than not are then identified as the noisy region, and transformed back into dimensional terms in order to generate the fried egg plot for the helicopter. Figure 7b shows this plot for the MD-902 estimated using data from all other helicopters in the database; the hashed noisy region is superimposed over the Ground Noise Exposure Levels contours from Figure 3b, and corresponds well to the noisy region of the operating envelope. The identified noisy region extends past the range of measured data for the helicopter in the low speed, high sink rate region of the envelope.

Random Forest

Another machine learning technique that was effectively applied to estimate the noisy region of a helicopter's operating envelope is the random forest classifier. The random forest model is an ensemble method, which blends the output of a number of decision tree classifiers that are each tuned to fit to the measured data. Figure 8 diagrams the first three of ten decision layers of one of the trees making up the random forest model constructed from the noise data (once again, excluding the MD 902). Each square block represents a "bin" of data, which may then be partitioned along a feature value according to the decision criterion shown in the diamond block below the source data block. Values that meet the criterion are included in the bin to the left of the decision criterion and those that are not are included in the bin to the right.

Each criterion used to divide the data is selected in order to reduce the overall Gini impurity index of the partitioned data from the source data. The Gini impurity index is a measure of the probability that a randomly selected member of the data set will be misclassified if the entire data set is classified with a probability distribution in proportion to the distribution of data contained within it, i.e.,

$$I_G = 1 - \sum_i p_i^2 \tag{10}$$

for the binary classification problem posed in this paper, the Gini index simplifies to $I_G = 2p_1p_2$.

If all of the data in a set are of the same class, the index reaches a minimum $I_G = 0$. Likewise, if half of the data belong to one class and half to the other, the index reaches a maximum of $I_G = 0.5$. Each split is chosen (Ref. 19) such that there is a net reduction of impurity:

$$I_{G_{True}} \frac{N_{True}}{N} + I_{G_{False}} \frac{N_{False}}{N} < I_G \tag{11}$$

In Figure 8, each data bin lists the impurity, I_G, of the data in that bin, the percentage of the total number of samples in the data set contained within that bin, and the percentages of data in that bin classified as noisy or not-noisy. In many cases, after several splits a pure ($I_G = 0$) partition is obtained and no more splits are required along that branch since all samples belong to the same class. If the maximum depth of the tree is reached (set to ten splits in this paper) before all bins are pure, the remaining impure bins will be assigned a probabilistic value according to the proportion of samples in each class in that bin. These residual probabilities can then be used to predict the probability of a noisy condition by following the criteria for any set of feature values.

The random forest is composed by generating a number of decision trees using a "bagging" technique, whereby each tree in the forest is generated from a randomly selected and permuted subset of the data points containing about two thirds of the total samples. The random forest classification probability is then the average probability predicted by all trees in the forest. The random forest model assessed in this paper is composed of ten different trees. Figure 9a shows the probability of a noisy condition for the MD-902, again compared against the classified data excluded from the modeling process. The high probability of noisy conditions region is accurately placed about the noisy data points, but has "blocky" shape because the decision criterion split along lines of constant feature value.

Figure 9b shows the corresponding estimate of the noisy region of the vehicle operating envelope again compared against the Ground Noise Exposure Level contours calculated for the vehicle. The model performs well in identifying the noisiest portion of the operating envelope, although the region does contain spurious details that do not correspond to the physical mechanisms of BVI noise.

One advantage of the random forest technique is that the details of the decision trees are accessible, which can provide some insight into how and why the model performs as it does. For example, Figure 10 plots the Gini importance of all five features derived from the decision trees. The Gini importance describes the relative effectiveness of decision criteria acting on the feature in reducing the Gini impurity over all of the decision trees in the ensemble model. Intuitively, the main rotor angle of attack, α, is by far the most important feature in the model due to the strong influence angle of attack has on BVI miss-distance and the resulting noise. The next most important feature is the main rotor advance ratio, μ. The remaining three features are relatively less important, and the specific rank order of these three parameters was observed to vary depending on the randomization of the data during model fitting.

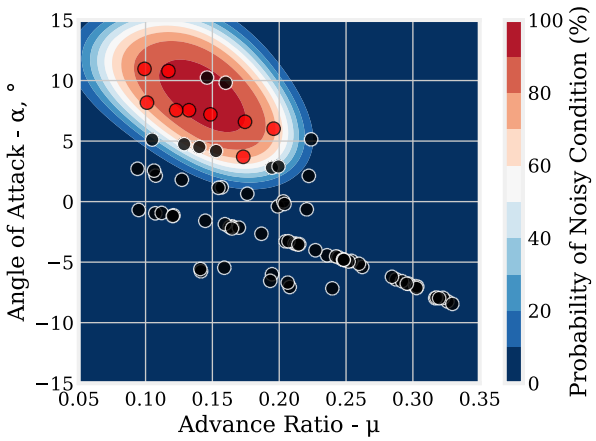

(a) Estimated probability of a noisy rotor operating condition. Measured flight conditions are marked with circles: black circles were identified as quiet and red circles as noisy. $C_W = 0.006$, $M_H = 0.61$, $N_b = 5$.

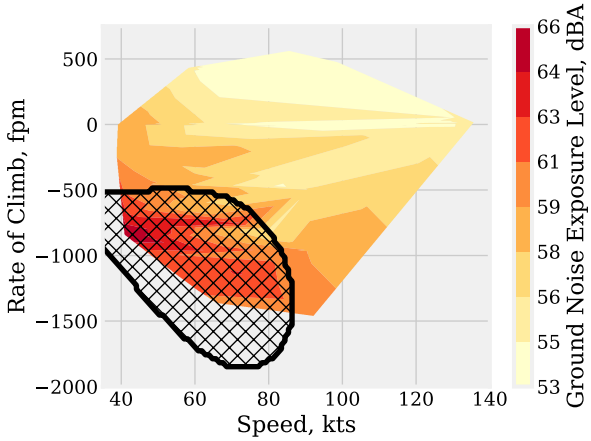

(b) Predicted noisy region (hashed) plotted over ground noise exposure level contours derived from measured data.

Fig. 7: Output of the Support Vector Classifier (SVC) model compared to measured data for the MD-902 as tested at Eglin AFB.

Multilayer Perceptron

The last method evaluated is the MultiLayer Perceptron (MLP) classifier, which is a class of feedforward artificial neural network where the neurons are organized into layers. A diagram of an MLP network is shown in Figure 11. The network propagates information from the input layer of feature values, through one or more "hidden layers," and finally to the output layer, which provides the classifier's output. The input to each neuron is a weighted sum of the outputs, ψ_j, of the previous layer:

$$x_i = \sum_j w_{ij} \psi_j \tag{12}$$

For the input layer, the outputs, ψ_j, are simply the scaled values of the five features. The classifier used in this paper has a single hidden layer of 100 neurons. The output of each neuron in the hidden layer is described by the rectified linear unit activation function, $\psi(x)$, which approximates the derivative of the logistic function.

$$\psi_i = \psi(x_i) = \max(0, x_i) \tag{13}$$

Finally, the output layer consists of a single neuron that provides a single output from the entire network with the "softmax" activation function:

$$\psi_i = \frac{\exp(x_i)}{\sum_k^N \exp(x_k)} \tag{14}$$

where there are $N = 100$ neurons in the preceding hidden layer. The softmax activation function limits the range of output values between zero and one, and is equivalent to the categorical probability distribution, i.e., the output of the network is the probability that the input condition is considered noisy.

To train the model, the weights w_{ij} are set for each layer to minimize the log loss error between model output and the training data set. Due to the simplicity of the activation functions, and the fact that activation in the hidden layer is sparse since the rectified linear unit function is often zero valued, this MLP classifier is relatively quick to train and evaluate.

Figure 12a plots the probability of noisiness for the MD-902 estimated by the MLP model trained to the database with the MD-902 data excluded. The MLP classifier performs well in identifying the region where noisy conditions exist; all nine noisy conditions are correctly classified and only two conditions are misclassified as noisy. Figure 12b plots the estimated noisy region over the ground noise exposure level contours for the MD-902. The output of the model is very similar to the SVM classifier evaluated in Figure 7b.

RESULTS

The modeling process was repeated for eight additional helicopters, with the helicopter removed from the database and the model retrained on the remaining data. Each model was then applied to predict the noisy region of the operating envelope for the helicopter excluded from the training dataset. The ground noise exposure level contours and noisy region identified by the MLP model for nine of the ten helicopters in the database are plotted in Figure 13. The AS350BA is excluded because only a limited number of conditions were tested, but across a wide range of density altitudes and vehicle gross weights. Similar results were achieved in all cases for the SVM classifier, much like the MD-902 examples shown previously. For that reason, these plots are not shown in this paper.

The model correctly identifies the noisy region of the operating envelope for each helicopter, despite the wide variation in helicopter rotor systems and configurations that cause the noisy region to vary between models. The helicopters with two bladed rotors—Figs. 13c, 13h, and 13i—have noisy operating regions that are largely confined to a certain range of speed and sink rate, somewhat like the canonical fried egg plot shown

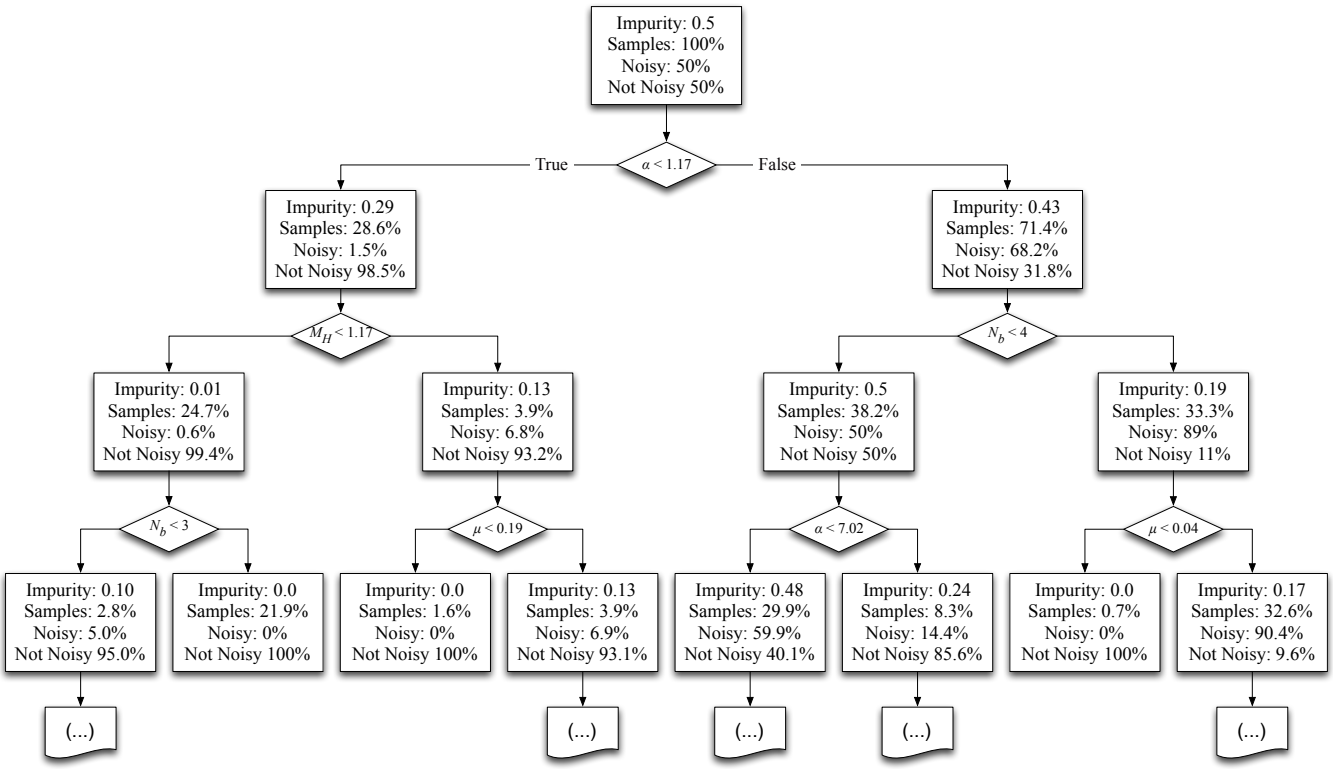

Fig. 8: Graph of the first three decision layers of one tree in the Random Forest model.

in Figure 1. However, the other helicopters with multibladed rotor systems exhibit high noise levels over a wide speed range, with the noisy region more aptly described as a "strip of bacon" than a "fried egg." This is most likely because the number of potential BVI events for a given advance ratio increases with the square of the number of blades, N_b^2, i.e., proportional to the number of blade – vortex pairs. This implies that while a two-bladed helicopter may be able to establish a speed corresponding to a rotor advance ratio where no single strong BVI is present at any rate of sink, rotor systems with many blades will have at least one strong BVI at some sink rate for every advance ratio. If those sink rates where BVI occur cannot be avoided, then it is important to pass through these conditions quickly, limiting the duration of BVI noise exposure.

The AS350B3 shown in Figure 13a was equipped for utility operations at the time of testing, including an externally mounted cargo basket. Using the drag estimation procedure described in Reference 7, the effective flat plate drag area of the B3 with the cargo basket was calculated to be 175% of that of the clean AS350BA previously measured during the NASA/Army Altitude Variation Tests described in 12. The effect of additional drag on noise can be examined in isolation by varying the drag of the helicopter in the noise abatement model and observing the trends in the estimated noisy region. Figure 14a plots the variation in the noisy region for the MD-902 MLP classifier at three different levels of the effective flat plate drag area, f, normalized by rotor area, A. As drag is increased, the noisy region is observed to shift to steeper descent rates. This shift is greatest at higher speeds, where the effects of drag on the rotor trim are greater.

This shift is explained because, to first order, the tip-path-plane angle of attack in steady flight is directly proportional to the change in the rotor drag to weight ratio:

$$\alpha = -\frac{f}{A}\frac{\mu^2}{2C_W} - \gamma \tag{15}$$

Therefore, a higher drag helicopter will operate at a lower tip-path-plane angle of attack for the same dimensionally defined speed and rate of sink, changing the operating point of the helicopter on Figure 12a. The helicopter would need to descend at a higher rate of sink, or more negative flight path angle, γ, to reach the same noisy operating region.

In addition to changes to the vehicle configuration, the noise radiation characteristics of the helicopter are influenced by the ambient atmospheric conditions (Ref. 7). Having been constructed on the basis of the nondimensional parameters that govern rotor noise, the machine learning classifier can account for changes in the noisy operating region caused by changes in ambient conditions caused by day-to-day variations, changes in geography and flight altitude. Figure 14b demonstrates this for the MD-902 subjected to International Standard Atmosphere (ISA) conditions at different altitudes above sea level. As altitude increases, the low speed portion of the noisy region drops to higher sink rates as reduced density causes the weight coefficient, C_W, to increase. This should be expected, since an increase in C_W will also increase the induced velocity through the rotor, causing BVI noise to occur at higher sink

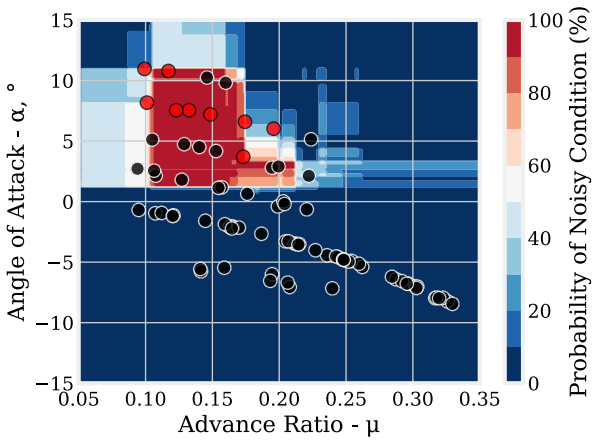

(a) Estimated probability of a noisy rotor operating condition. Measured flight conditions are marked with circles: black circles were identified as quiet and red circles as noisy. $C_W = 0.006$, $M_H = 0.61$, $N_b = 5$.

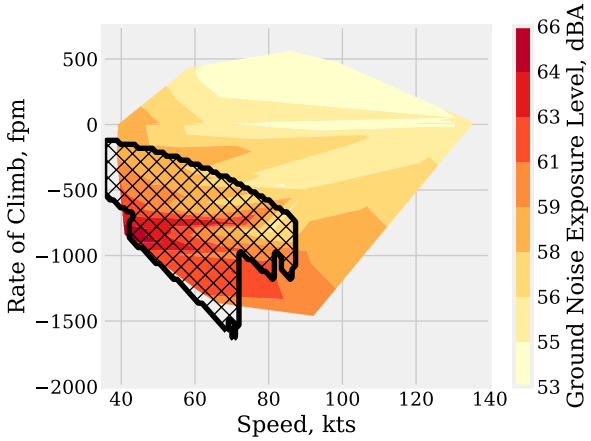

(b) Predicted noisy region (hashed) plotted over ground noise exposure level contours derived from measured data.

Fig. 9: Output of the Random Forest (RF) model compared to measured data for the MD-902 as tested at Eglin AFB.

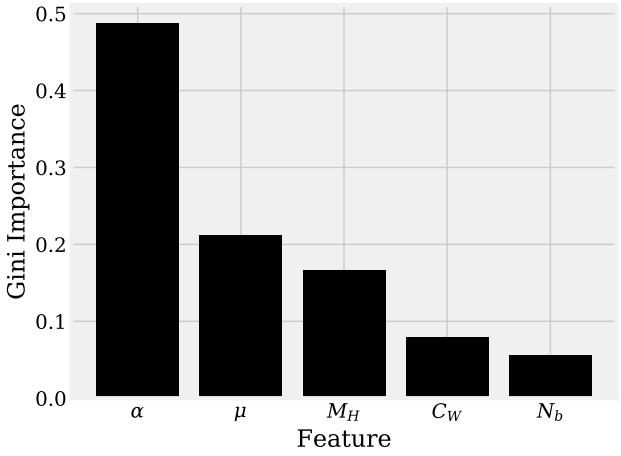

Fig. 10: Gini importance of features to "noisiness" classification identified by the Random Forest model.

rates, especially at low airspeed. The region enlarges with increasing altitude, due to the increase in hover tip Mach number, M_H, with decreasing air temperature. Also, the region extends to higher speeds with increasing altitude because of the increase in advance ratio, μ, with decreasing density for the same calibrated airspeed, further increasing the advancing tip Mach number of the rotor.

LIMITATIONS OF EMPIRICAL MODELING

The models developed in this paper have been shown to have the accuracy required for estimating useful noise abatement information across a range of helicopters operating in different configurations and ambient conditions. However, there are several potential limitations to this modeling approach that should be considered when applying it:

- Due to the empirical nature of machine learning, the resulting models may produce inaccurate results when extrapolated far outside the range of measured data, for instance if applied to helicopters much heavier than the light to medium helicopters represented in the present database or in ambient conditions well outside the range of measured values. This problem might be addressed most effectively by incorporating data from wind tunnel measurements where much wider variations in the rotor operating condition can be measured. The dataset might also be augmented with measured data for additional helicopters or well-calibrated computational models of helicopter BVI noise.

- The noise data used to train the models developed in this paper only contain measurements of helicopters with conventional rotor systems. Measurements of more exotic rotor designs with extensive anhedral, sweep, or highly nonlinear twist distributions may not generalize as well across rotor designs. However, the limited nearfield acoustic data presented for the Blue Edge rotor (Ref. 20)—having anhedral tips and a highly swept planform designed to reduce BVI—indicate that although noise levels at any particular operating condition may vary with such rotor design changes, the regions of the operating envelope where BVI occurs does not change significantly.

- The definition of a noisy operating condition used in the paper is a simple heuristic that does not map directly to the physical mechanisms of BVI noise, and therefore, is prone to contamination by other noise sources, such as High Speed Impulsive (HSI) or tail rotor noise sources. These sources may not vary with the selected features in the same way. The robustness and accuracy of the model might be further improved by developing a noise metric based on a technique that isolates the contributions of

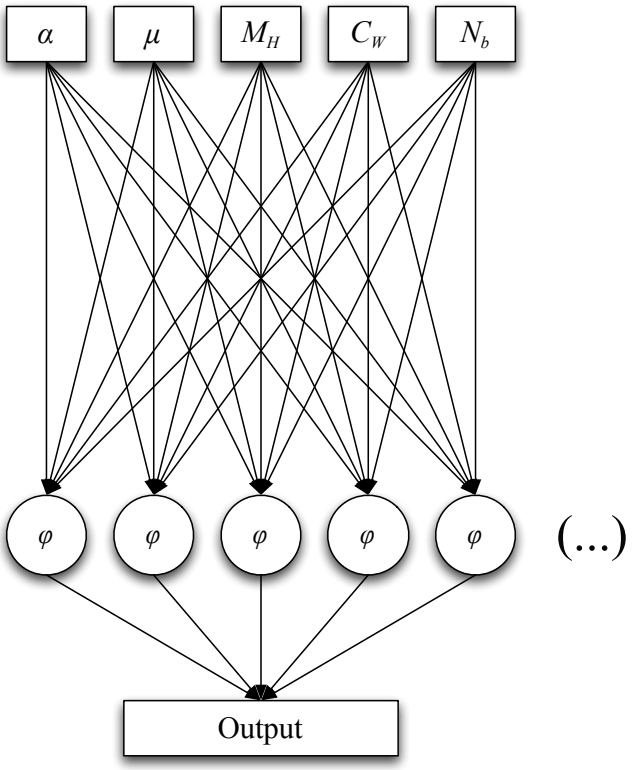

Fig. 11: Diagram of the multilayer perceptron network used in this paper.

BVI and other noise sources, such as the BVI extraction proposed by Stephenson in Ref. 21.

CONCLUSIONS

A method of generating empirical models capable of identifying the noisy operating conditions of helicopters for which no measured data are available was developed and demonstrated in this paper. The method combines machine learning techniques with the principle of nondimensionalization to allow the measured data to be generalized between different helicopters. Several different machine learning techniques were assessed; both Support Vector Machine (SVM) and MultiLayer Perceptron (MLP) classifiers were found to achieve good performance in identifying the noisy region of a helicopter's operating envelope, while the Random Forest technique additionally provides some insight to the relative importance of different attributes to the occurrence of BVI. The models were applied to predict the noisy operating region for ten different helicopters that had been experimentally measured. Noise abatement plots identifying the noisy region were estimated with good accuracy shown in all cases. The ability of the model to provide noise abatement information specific to the configuration of an individual vehicle and the ambient conditions in which it operates was also demonstrated. The modeling method developed in this paper shows promise as a "universal" method of generating useful noise abatement information for all types of conventional helicopters in service.

ACKNOWLEDGMENTS

The author would like to acknowledge the significant contribution to this research of Charles D. Smith, Analytical Mechanics Associates, for developing the extensive database of RNM/ART helicopter source noise hemispheres from which the model described in this paper was developed, as well as Menachem Rafaelof, National Institute of Aerospace, for helpful discussions and advice on the applications of decision tree models. The author would also like to thank Michael E. Watts, NASA Langley Research Center, and Dr. James H. Stephenson, US Army Aviation Development Directorate, for their insightful suggestions to improve this paper.

REFERENCES

[1]"LA Helicopter Noise Initiative," `http://heli-noise-la.com`, Accessed: 2017-03-05.

[2]"Westchester County Airport Noise Abatement," `http://airport.westchestergov.com/environmental-management-system/noise-abatement`, Accessed: 2017-03-05.

[3]"NYCEDC And Helicopter Tourism & Jobs Council Announce New Measures to Reduce Helicopter Noise And Impacts Across New York City," `https://www.nycedc.com/press-release/nycedc-and-helicopter-tourism-jobs-council-announce-new-measures-reduce-helicopter`, Accessed: 2017-03-05, February 2016.

[4]Helicopter Association International Fly Neighborly Committee, *Fly Neighborly Guide*, Helicopter Association International, 2007.

[5]Schmitz, F. H., Greenwood, E., Sickenberger, R. D., Gopalan, G., Sim, B. W.-C., Conner, D. A., Moralez, E., and Decker, W., "Measurement and Characterization of Helicopter Noise in Steady-State and Maneuvering Flight," American Helicopter Society 63rd Annual Forum, May 2007.

[6]Greenwood, E. and Schmitz, F. H., "The Effects of Ambient Conditions on Helicopter Rotor Source Noise Modeling," *AIAA Journal of Aircraft*, Vol. 51, (1), 2014, pp. 90–103.

[7]Greenwood, E., Sim, B., and Boyd, D., "The Effects of Ambient Conditions on Helicopter Harmonic Noise Radiation: Theory and Experiment," American Helicopter Society 72nd Annual Forum, May 2016.

[8]Lucas, M. J. and Marcolini, M. A., "Rotorcraft Noise Model," AHS Technical Specialists' Meeting for Rotorcraft Acoustics and Aerodynamics, October 1997.

[9]Conner, D. A. and Page, J. A., "A Tool for Low Noise Procedures Design and Community Noise Impact Assessment: The Rotorcraft Noise Model (RNM)," Heli Japan, 2002.

[10]Watts, M. E., Conner, D. A., and Smith, C. D., "Joint Eglin Acoustic Week III Data Report," Technical Report TM-2010-216206, NASA, March 2010.

[11]Watts, M. E., Greenwood, E., Smith, C. D., Snider, R., and Conner, D. A., "Maneuver Acoustic Flight Test of the Bell 430 Helicopter Data Report," Technical Report TM–2014-218266, NASA, 2014.

[12]Watts, M. E., Greenwood, E., Sim, B. W., Stephenson, J. H., and Smith, C. D., "Helicopter Acoustic Flight Test with Altitude Variation and Maneuvers," Technical Report TM-2016-219354, NASA, December 2016.

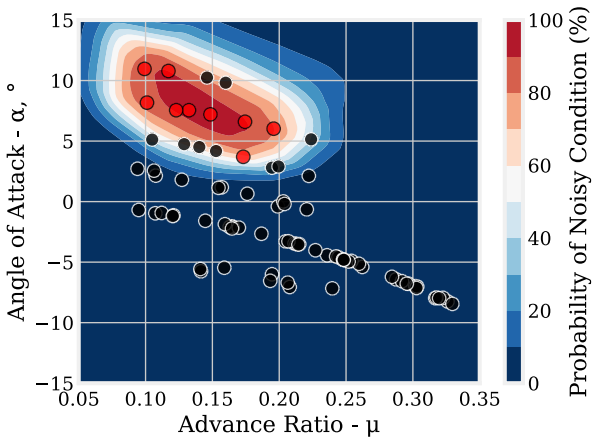

(a) Estimated probability of a noisy rotor operating condition. Measured flight conditions are marked with circles: black circles were identified as quiet and red circles as noisy. $C_W = 0.006$, $M_H = 0.61$, $N_b = 5$.

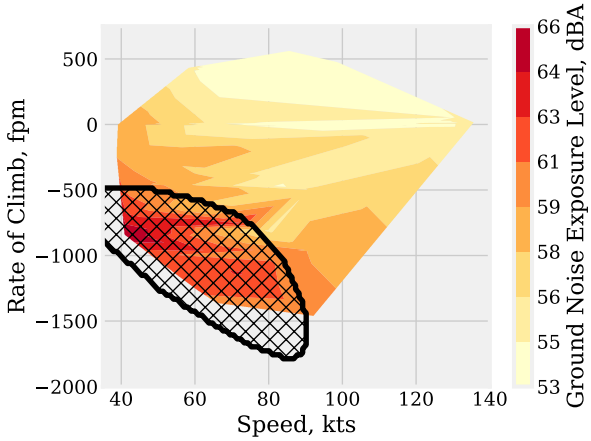

(b) Predicted noisy region (hashed) plotted over ground noise exposure level contours derived from measured data.

Fig. 12: Output of the Multi-Layer Perceptron (MLP) model compared to measured data for the MD-902 as tested at Eglin AFB.

[13]Boxwell, D. A., Schmitz, F. H., Splettstoesser, W. R., and Schultz, K. J., "Helicopter Model Rotor-Blade Vortex Interaction Impulsive Noise: Scalability and Parametric Variations," *Journal of the American Helicopter Society*, Vol. 32, (1), 1987, pp. 3–12.

[14]Chawla, N. V., Bowyer, K. W., Hall, L. O., and Kegelmeyer, W. P., "SMOTE: Synthetic Minority Over-sampling Technique," *Journal of Artificial Intelligence Research*, Vol. 16, 2002, pp. 321–357.

[15]Pedregosa, F., Varoquaux, G., Gramfort, A., Michel, V., Thirion, B., Grisel, O., Blondel, M., Prettenhofer, P., Weiss, R., Dubourg, V., Vanderplas, J., Passos, A., Cournapeau, D., Brucher, M., Perrot, M., and Duchesnay, E., "Scikit-learn: Machine Learning in Python," *Journal of Machine Learning Research*, Vol. 12, 2011, pp. 2825–2830.

[16]Cortes, C. and Vapnik, V., "Support-vector networks," *Machine Learning*, Vol. 20, (3), Sep 1995, pp. 273–297. doi: 10.1007/BF00994018

[17]Gunn, S. R., "Support vector machines for classification and regression," *ISIS Technical Reports*, Vol. 14, 1998, pp. 85–86.

[18]Platt, J. C., "Probabilistic Outputs for Support Vector Machines and Comparisons to Regularized Likelihood Methods," Advances in Large Margin Classifiers, 1999.

[19]Breiman, L., Friedman, J. H., Olshen, R. A., and Stone, C. J., *Classification and Regression Trees*, Statistics/Probability Series, Wadsworth Publishing Company, Belmont, California, U.S.A., 1984.

[20]Gervais, M. and Gareton, V., "Analysis of Main Rotor Noise Reduction Due to Novel Planform Design - The Blue Edge Blade," 37th European Rotorcraft Forum, September 2011.

[21]Stephenson, J. H. and Tinney, C. E., "Extracting Blade-Vortex Interactions Using Continuous Wavelet Transforms," *Journal of the American Helicopter Society*, Vol. 62, (2), 2017, pp. 1–10. doi: 10.4050/JAHS.62.022001

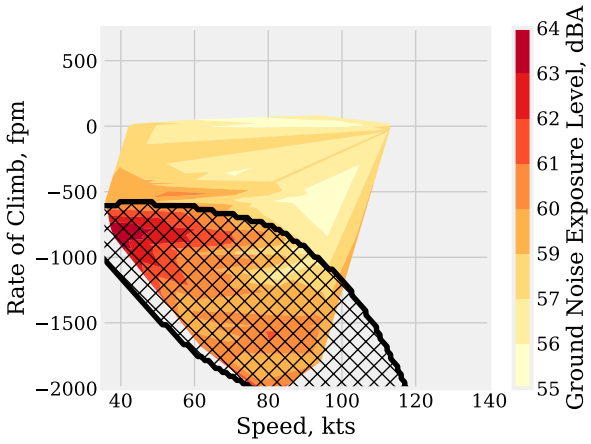

(a) Airbus AS350B3 (with basket) at Amedee AAF.

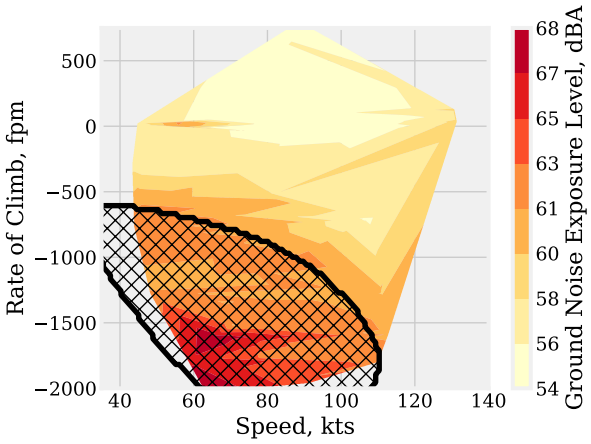

(b) Airbus EC130B4 at Amedee AAF.

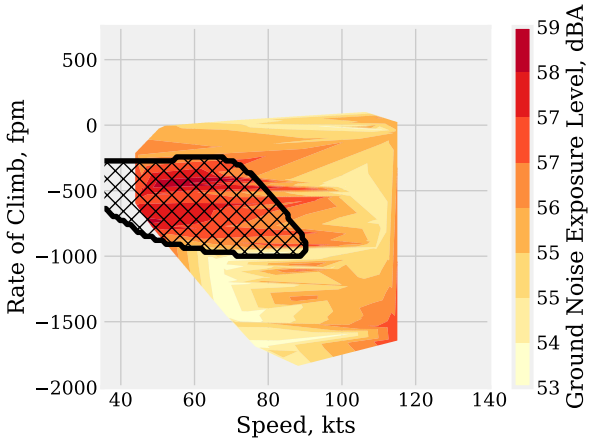

(c) Bell 206L3 at Amedee AAF.

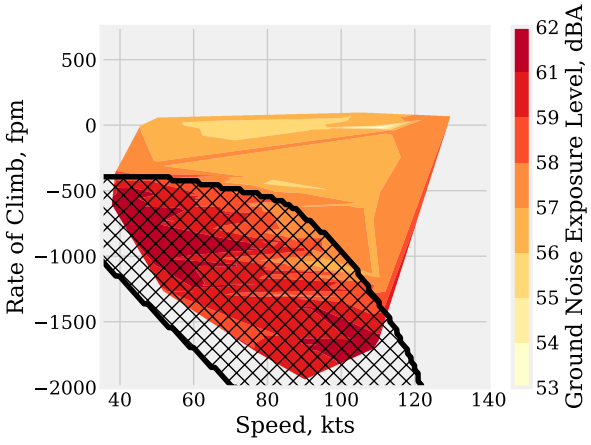

(d) Bell 407 at Amedee AAF.

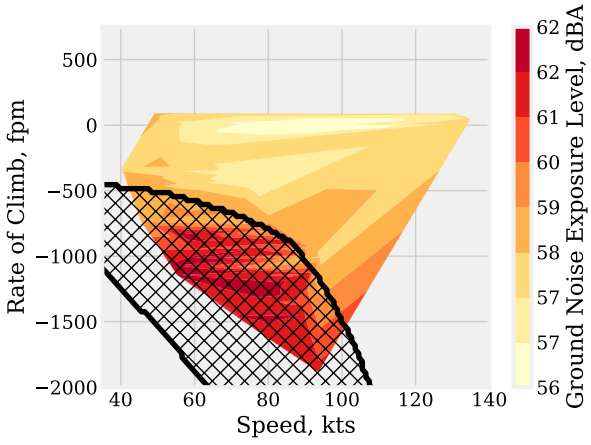

(e) Bell 430 at Eglin AFB.

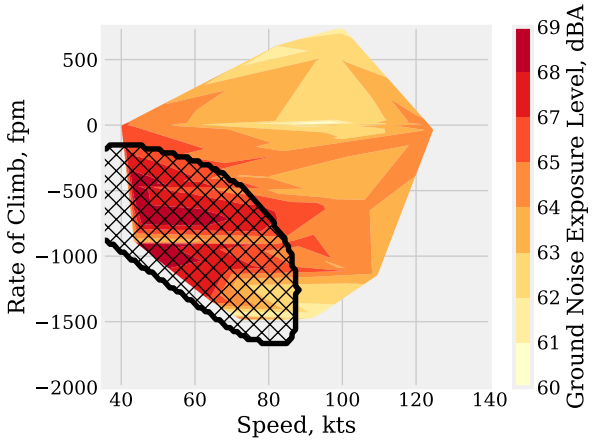

(f) Mil Mi-17 at Eglin AFB.

Fig. 13: Ground noise exposure level contours as a function of flight condition. Scale varies between aircraft. noisy conditions identified by MLP classifier overlayed in hashed region. Continues on next page.

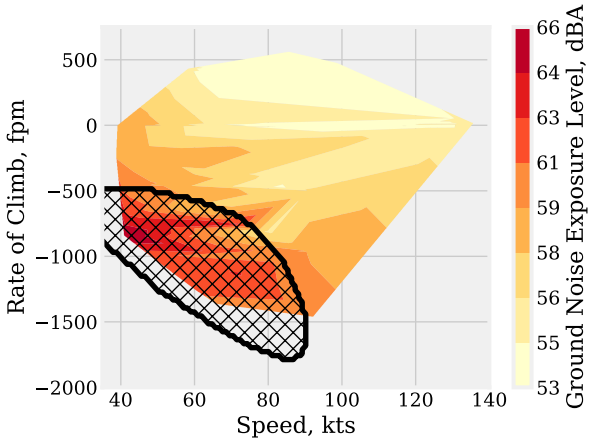

(g) MD Helicopters MD902 at Eglin AFB.

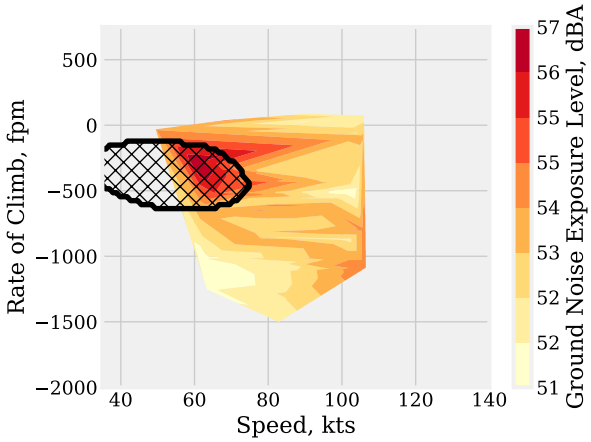

(h) Robinson R-44 at Eglin AFB.

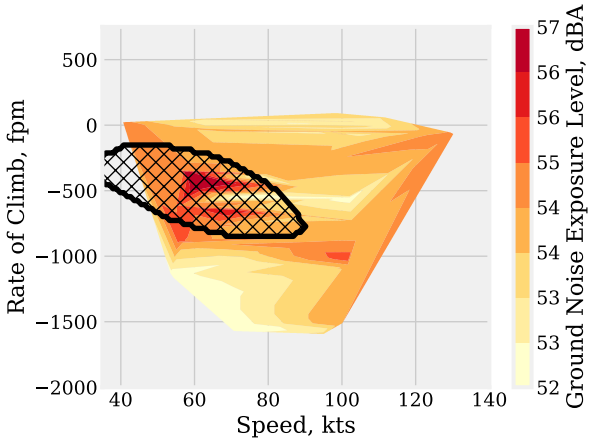

(i) Robinson R-66 at Eglin AFB.

Fig. 13: Ground noise exposure level contours as a function of flight condition. Scale varies between aircraft. noisy conditions identified by MLP classifier overlayed in hashed region.

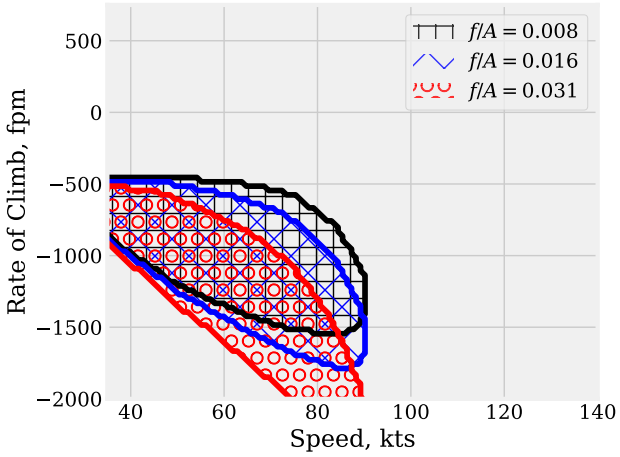

(a) Various effective flat plate drag areas.

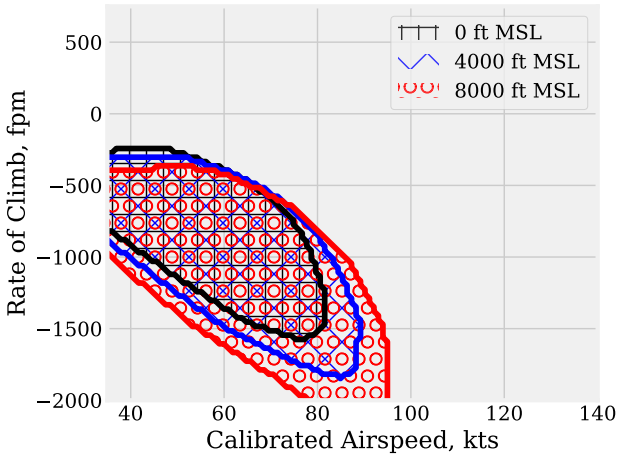

(b) Various altitudes above Mean Sea Level (MSL) under International Standard Atmosphere ambient atmospheric conditions.

Fig. 14: Estimation varitions in the noisy region using the MLP model for the MD-902 under different operating conditions.